# Conformal mapping on rough boundaries. I. Applications to harmonic problems

Damien Vandembroucq and Stéphane Roux
*Laboratoire de Physique et Mécanique des Milieux Hétérogènes, Ecole Supérieure de Physique et de Chimie Industrielles, 10 rue Vauquelin, 75231 Paris Cedex 05, France*

(Received 29 January 1996; revised manuscript received 16 December 1996)

The aim of this study is to analyze the properties of harmonic fields in the vicinity of rough boundaries where either a constant potential or a zero flux is imposed, while a constant field is prescribed at an infinite distance from this boundary. We introduce a conformal mapping technique that is tailored to this problem in two dimensions. An efficient algorithm is introduced to compute the conformal map for arbitrarily chosen boundaries. Harmonic fields can then simply be read from the conformal map. We discuss applications to ''equivalent'' smooth interfaces. We study the correlations between the topography and the field at the surface. Finally we apply the conformal map to the computation of inhomogeneous harmonic fields such as the derivation of Green function for localized flux on the surface of a rough boundary. [S1063-651X(97)03205-4]

PACS number(s): 02.70.−c, 66.10.Cb, 44.30.+v, 61.43.Hv

## I. INTRODUCTION

Defining and computing effective properties of heterogeneous media is a subject that has been studied for a long time, and for which a number of powerful techniques have been developed. In most cases, however, the heterogeneities are considered to lie in the bulk of the material. Another type of inhomogeneity is due to the random geometry of the surface on which boundary conditions are applied. This study focuses on this second type. We will thus consider homogeneous media that are limited by a rough surface or interface. Our purpose here is to introduce a very efficient way of solving harmonic problems in two-dimensional systems for any geometry of the boundary.

The occurrence of rough interfaces in nature is more the general rule than the exception. Apart from very specific cases such as mica where a careful cleavage can produce planar surfaces at the atomic scale, surfaces are rough. Even glass with a very homogeneous composition, where the surface is obtained by a slow cooling of the material, so that surface tension can act effectively to smoothen all irregularities, displays roughness in the range 5–50 nm over a window of a few micrometers width [1]. Similarly, the so-called ''mirror'' fracture surface that is optically smooth exhibits specific topographic patterns when examined with an atomic force microscope [2]. The key question is thus how to identify the relevant range of scales at which roughness appears. From common observations, this question may not have a simple clear cut answer. Indeed, in a variety of cases, the amplitude of the roughness appears to be strongly dependent on the size of the examined surface. A particular class of such scale dependent roughness, namely, self-affine roughness [3,4], has recently motivated a lot of activity (see Refs. [5–7] for recent reviews) because of both its relevance in many different instances, and its theoretical justification, which has been obtained in statistical physics for a wide class of models, such as growth models [8], molecular beam epitaxy [9], fracture surfaces [10], and immiscible fluid interfaces [11]. Although the present study is not specific to self-affine surfaces, we shall consider this particular class in order to apply our method. The interest in this choice may be explained by the following: (i) the description of the roughness is realistic for a number of applications, (ii) the consequences can be expressed in quite general terms as a function of a few parameters directly accessible experimentally, and finally (iii) the most commonly studied roughness models are ''monochromatic'' surfaces with a single asperity pattern repeated periodically, and hence the transposition to more complex geometries may be wrong (examples of such cases will be discussed below).

As previously mentioned, if most surfaces are rough, this roughness may be of small amplitude macroscopically, and thus one may feel that its role can be neglected in most cases. Fortunately, this is generally true. Taking into account precisely the surface roughness may be required in two distinct classes of problems.

The first class (I) covers applications where the roughness cannot be neglected at the scale at which the bulk field varies. For obvious reasons, there is no way to avoid an accurate description of the boundary. We may mention the following potential applications:

(1) In confined geometries, such as those encountered naturally in surface force study, the roughness of the surface may affect the interpretation and thus the precision of the measurements since the distance between two facing surfaces is generally estimated from indirect measurements of transport in the gap between the surfaces [12].

(2) Fields that are rapidly varying in space will be sensitive to fine details of the boundary geometry. The most obvious example in this field is the reflection and scattering of a wave by a rough boundary [13]. Of particular importance are the cases of surface waves, evanescent waves, Rayleigh waves in elasticity, etc.

(3) In a similar spirit, diffusion processes may display anomalous behaviors at short times where the diffusion length is smaller than or comparable to the roughness [14].

The second class of problems (II) where roughness cannot be neglected is when one has to focus on the boundary, either because only this part matters for extraneous reasons or because the system is sensitive to high fields that can be induced by the roughness itself. Some examples of these two cases are as follows: (i) Surface phenomena such as electro-

 

filtration require a proper solution of, say, a Stokes flow field, in the immediate vicinity (typically Debye length scale) of a rough boundary where an electric boundary layer is present and can be entrained by the fluid to give rise to an electric current in response to a fluid flow in a porous medium [15]. (ii) The brittle fracture of glass is generally due to surface defects that induce locally high stresses, which reduce significantly the breaking limit of this material. In the absence of specific surface degradation the most important source of surface defects is the topography itself [16]. (iii) Some growth models have a local growth rate that depends on a harmonic field locally. The development of unstable modes that will finally induce a macroscopic roughening requires the proper analysis of the field at the surface [4,8].

The relative independence of the bulk field on the small scale roughness of the boundary for a slowly varying field (class II problems) can be used to explore the local field close to the boundary using an asymptotic analysis with a double scale technique. The large scale problem consists in solving the problem at hand by replacing the rough boundary by a smooth equivalent one. The small scale problem deals with the details of the rough boundary and matches at ''infinity'' with a homogeneous field. This local problem will be considered in full detail in the following.

These examples are obviously not exhaustive. Inhomogeneous boundary conditions may arise, for instance, in contact problems where the roughness cannot be neglected [17,18]. One may also consider application outside the realm of physical applications, such as the use of harmonic problems and particularly conformal maps as a simple means of meshing a domain limited by a rough boundary.

In the present paper we essentially focus on harmonic problems. The latter arise in a variety of different domains in physics, such as electrostatics, thermal or concentration diffusion, flow in porous media, and antiplane elasticity, to mention a few. This field has been intensively studied in the last decade and special attention has focused on the ''constant phase angle'' behavior encountered for the measured impedance of rough electrodes. Taking advantage of the formal equivalence between electrostatics and stationary diffusion processes, several authors have developed random-walk algorithms [19–22] eventually improved by coarse-graining techniques [23] that allowed for a better comprehension of this complex phenomenon and its dependence on the statistical properties of the surface.

The random-walk–based computation provides a general way of addressing harmonic problems. There are very few limitations to the method in terms of space dimensionality or constraints on the roughness, in contrast to most other methods. This implies that this method is extremely well suited to extremely rough, or fractal boundaries. It is extremely easy to get a rough estimate of global quantities such as electrical impedance. The drawback of this method is, however, its precision. Based on random walks, the convergence of the results will be extremely slow, typically involving factors of order $1/\sqrt{N}$ where $N$ is the number of walkers.

The most common numerical methods to study harmonic fields are finite-element or finite-difference schemes. The latter are, however, rather inefficient in our case since one has to solve a two-dimensional problem. A more clever way is to use a boundary integral formulation, leading to boundary element numerical implementation. This technique is extremely well suited to our problem, but rather delicate to use, because of the use of singular influence functions between elements.

The method we introduce here shares a number of advantages with the boundary element algorithm in the sense that only surface degrees of freedom are taken into account. It thus has a fast convergence, and does not require a large memory. However, in contrast with the previous method, no singular elements are introduced, but rather simple evanescent wave modes. The practical implementation of the algorithm solely involves recursive calls to fast Fourier transform methods, with no special tricks. The convergence rate is exponential down to machine precision, thus allowing for arbitrary accuracy in short computation times. Moreover, the first steps of the algorithms can be performed analytically, providing a tool to access analytical results in a perturbation approach. Let us note also that this technique can be extended to all sorts of boundary conditions, source and sink distributions, etc. once the mapping has been obtained. It can also be applied to singular problems, such as, e.g., the determination of the stress intensity factor in a rough mode III crack in antiplane elasticity. It can also be extended to biharmonic problems as discussed in a companion paper [24].

Finally, let us stress that, besides physical problems, the algorithm may be interesting for numerical purposes. If one has to deal with a rough boundary, it might be convenient to use the conformal map simply to generate a regular meshing on which a finite-difference or finite-element method can be applied. The computation time needed to get the mapping is a simple small overhead computation time.

Beyond the harmonic problems, another use of conformal mappings is the resolution of biharmonic problems near a rough interface; both stress field in elasticity and velocity field in low Reynolds number fluid mechanics [25–29] can be derived from potentials that obey such bi-Laplacian equations. We refer the reader to the companion paper [24], which is completely devoted to this specific problem.

This paper is devoted to the study of harmonic problems in two-dimensional (2D) semi-infinite media limited by a rough boundary. To extend the definition of the profile of the boundary to infinity, we use periodic boundary conditions along the boundary. Although very specific, this type of geometry will be very convenient as soon as no other boundary lies close to the first one. The distance threshold to consider in such a case is typically of the order of magnitude of the larger spatial wavelength of the profile, i.e., the spatial period in the geometry we have described. We use a conformal mapping technique. It consists of constructing a map from the domain of interest (in the complex plane) onto a regular semiplane. The conformity of the map allows one to preserve harmonicity through the map transform.

In a first part of this paper, we define the form of the conformal mapping suited to our geometry. Then, we address the problem of constructing the mapping associated with any prescribed interface. We show that this problem can be solved with an iterative algorithm using fast Fourier transforms (FFT). This algorithm allows one to get the conformal map in a few iterations of FFT, whose computation time scales as $N \ln(N)$, where $N$ is the number of Fourier modes used to describe the interface. Note the remarkable efficiency

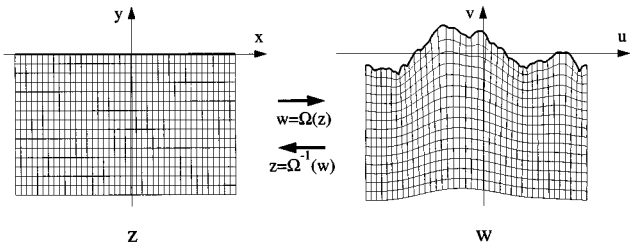


FIG. 1. A schematic illustration of the mapping $\Omega$, which maps the semi-infinite plane $\mathcal{D}$ onto the domain limited by a rough interface $\mathcal{E}$.

of such a technique, considering that the map gives the solution of a Laplacian field in the entire two-dimensional problem. This problem is very close to the so-called ''Theodorsen problem'' [30] in a circular geometry. We also show that one can generate maps that naturally give rise to self-affine boundaries, a powerful technique to explore generic properties of such problems. Specific applications of this technique to a self-affine profile are studied, which includes (i) the question of defining an equivalent smooth (planar) interface, and finding its height compared to the geometrical average height of the interface, and (ii) the correlation between the height and the field, which is computed exactly in the limit of a small roughness amplitude. These two examples demonstrate the unexpected difference in behaviors for persistent and antipersistent profiles. Finally, we give the expression of the Green function for localized flux on a rough interface.

## II. SUITED CONFORMAL MAPPING

### A. Notations

In order to study harmonic fields in two dimensions, very powerful techniques have been developed based on complex analysis [30]. Among these, we will use in the following conformal maps, which allow one to relate the geometry we wish to study (i.e., a semi-infinite domain limited by a rough interface), to a regular one as schematically illustrated in Fig. 1.

As usual, we will identify a point in the plane $(x,y)$ with the complex number $z=x+iy$. We note $\overline{z}=x-iy$ the complex conjugate of $z$. The two variables $z$ and $\overline{z}$ can be treated as independent variables instead of $x$ and $y$. A mapping from the complex plane onto itself is simply defined as a complex function $\Omega$ of $z$ and $\overline{z}$, which transforms one point of the complex $z$ plane into another point $\Omega(z,\overline{z})$. For the mapping to be of physical interest it has to be bijective in a domain of interest, and thus inversible. The mapping is *conformal* if the function is *holomorphic*; i.e., it depends only on $z$ and not on $\overline{z}$. It can be shown that in this case, local angles are preserved in the transformation—apart from singular points—and hence the term ''conformal.'' Moreover, the real part and the imaginary part of any such holomorphic function are both harmonic, i.e., $\nabla^2\mathrm{Re}\Omega=\nabla^2\mathrm{Im}\Omega=0$. The latter property results from the expression of the Laplacian operator in terms of the variables $z$ and $\overline{z}$:

$$\nabla^2\equiv\partial_{xx}^2+\partial_{yy}^2=4\partial_{z\overline{z}}^2. \tag{1}$$

Two obvious choices are well suited for our geometry: (i) a semi-infinite plane $\mathcal{D}$, $\mathrm{Im}(z)\leqslant 0$ and (ii) the unit circle $\mathcal{C}$, $|z|\leqslant 1$. These two domains can be related by the transformation $z\rightarrow\ln(z)$, and thus they are basically equivalent. Since the boundary we consider is periodic in the $x$ direction, the mapping to the unit circle is well suited. However, in the following, we will rather use the mapping to the half plane, since it corresponds directly to the ''reference'' problem where the roughness vanishes.

### B. Specific transformations

The domain of interest, denoted by $\mathcal{E}$, is limited by a rough interface $\partial\mathcal{E}$, which is a periodic function of $\mathrm{Re}(z)$ of period $X$. The conformal map $\Omega$ is a function of $z$, which associates one point of the reference domain, $\mathcal{D}$ or $\mathcal{C}$, to another point in $\mathcal{E}$. From now on in order to distinguish the initial and the image domain, we will denote a point in the image plane as $w=u+iv$, and keep the notation $z=x+iy$ for the initial plane unless otherwise mentioned. Before specifying the particular form of the boundary, it is possible to guess an adequate form for these transformations.

Let us first consider the mapping from the half plane $\mathcal{D}$ to $\mathcal{E}$. As $\mathrm{Im}(z)$ tends to $-\infty$, the mapping should approach the identity $\Omega(z)\rightarrow z$, since the roughness of the boundary is not expected to play any significant role at a large distance (compared to the period $X$) from the boundary. We introduce the function $\omega(z)$ such that

$$\Omega(z)=z+\omega(z). \tag{2}$$

Functions of the form $\exp(-ikz)$ with $k$ real thus appear to be natural candidates for $\omega(z)$. They are indeed periodic functions of $\mathrm{Re}(z)$, and vanish exponentially as $\mathrm{Im}(z)$ goes to $-\infty$ when $k>0$. Moreover, in order to satisfy the same periodicity as $\partial\mathcal{E}$ we require that $kX=2n\pi$, where $n$ is an integer. Thus we propose the following decomposition as an expression for the transformation $\Omega$;

$$\Omega(z)=z+\sum_{k=0}^{\infty}\omega_k e^{-2i\pi kz/X}. \tag{3}$$

Without loss of generality we will set $X=2\pi$ for the remainder of this paper.

The rough boundary is to be identified with the image of the $x$ axis, so that $\partial\mathcal{E}$ obeys the parametric equations

$$u=x+\mathrm{Re}\left(\sum_k \omega_k e^{-ikx}\right),$$

$$v=\mathrm{Im}\left(\sum_k \omega_k e^{-ikx}\right). \tag{4}$$

The corresponding transformation from the unit disk $\mathcal{C}$ to the domain $\mathcal{E}$ can be obtained from the above form (3) and the transformation from the disk to the semi-infinite plane $\mathrm{Im}z\leqslant 0$. The resulting transformation reads

$$\Omega(z)=i\,\ln(z)+\sum_k \omega_k z^k, \tag{5}$$

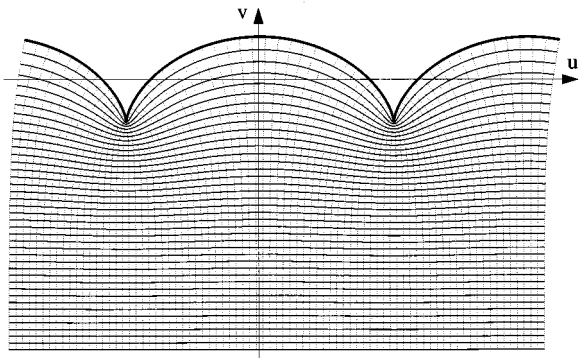


FIG. 2. Image of a regular square grid of the semi-plane $\mathcal{D}$ using the transformation (7). The parameter $\omega$ has been set to its maximum value of 1. A cusp appears on the boundary.

where $X=1$ has been used. Evidently, the image of the unit circle $z=e^{i\theta}$ provides the same parametric form as Eq. (4).

With the form of the transformation being imposed, one needs to check that the transformation is bijective: a point should have a single image, and an image point a unique parent. This condition imposes some restriction on the transformation $\Omega$. It can be rephrased simply for the transformation (3) as

$$\left|\frac{d\Omega}{dz}\right|_{z=x+iy} > 0 \tag{6}$$

for all $y<0$. In principle, it is sufficient to impose this condition only in the strict interior of the domain. If $d\Omega/dz=0$ on the boundary, a kink may appear at this point. In the following, we will assume that the interface is smooth at a small scale so that poles are forbidden on the boundary.

As an example, if the transformation is simply

$$\Omega(z)=z+\omega e^{-iz} \tag{7}$$

then the condition (6) reduces to $|1+i\omega e^{ix}e^{y}|>0$ or $|\omega|<1$. For this maximum value, the image of the $x$ axis is a cycloid, with cusp points. Figure 2 illustrates this limit case.

## III. COMPUTING THE MAPPING FOR AN IMPOSED INTERFACE

The above presented transformation is only useful for a particular application if the transformation $\Omega$ can be computed, once the boundary $\partial\mathcal{E}$ is imposed. This section is devoted to this problem. The algorithm that we have developed generates the transformation very efficiently. Different numerical techniques applied to computing the map from arbitrary closed domains to the unit disk can be found in Ref. [31]. Our algorithm can be shown to be related to the Jacobi method used in these studies.

### A. Description of the algorithm

We define the rough boundary $\partial\mathcal{E}$ as a single-valued real function $h$ such that $v=h(u)$ is the equation of the boundary. In other words, the boundary is given by the parametrized form $w=u+ih(u)$. To comply with the framework we have chosen here, we use in the following a $2\pi$ periodic $h$.

From the particular form of the transformation $\Omega$, we expand the real and imaginary parts on the boundary $\partial\mathcal{E}$:

$$\begin{aligned} u &= x+\mathrm{Re}\left[\sum_k \omega_k e^{-ikx}\right], \\ h(u) &= \mathrm{Im}\left[\sum_k \omega_k e^{-ikx}\right]. \end{aligned} \tag{8}$$

If $u$ were equal to $x$, the second equation would be close to a Fourier-transform expression of the function $h$. More precisely, rewriting the last equation as

$$h(u)=\mathrm{Re}\left[\sum_k i\overline{\omega_k}e^{ikx}\right] \tag{9}$$

we see that the coefficient $i\overline{w_k}$ can be computed from the Fourier transform of $h(u(x))$. The difficulty is that $u(x)$ is *a priori* unknown. However, we note that if the roughness is small enough, say of order $\epsilon$, $u$ can be written as $u=x+O(\epsilon)$. Therefore, identifying $x$ with $u$ is a zeroth-order approximation. From the latter, the coefficient $\omega_k$ can be computed by the Fourier transform of $h(u)$. This provides a first-order approximation of $u(x)$, from which an improved estimate of $\omega_k$ can be obtained by taking the Fourier transform of $h(u(x))$, i.e., a nonuniform sampling of the profile $h$. Iterating this scheme is the basis of our algorithm. We will omit for the time being the prerequisite on the amplitude of the roughness. We will return to this point by considering the stability of the algorithm.

The intermediate quantities appearing at the $k$th iteration will be labeled with a superscript $(k)$. We also formulate the algorithm directly in discrete terms suited for a numerical implementation. In the remainder of this paper, all functions will be decomposed over a set of $2n$ discrete values. The number of Fourier modes will thus be limited to $2n$. We first introduce a series of sampling points $u_j^{(k)}$ with $j=0,\ldots,n-1$, which is initially set to an arithmetic series $u_j^{(0)}=j\pi/n$. The sampling of $h(u)$ by $u_j^{(k)}$ gives the array

$$h_j^{(k)}=h(u_j^{(k)}). \tag{10}$$

The discrete Fourier transform of this array is the complex-valued array

$$a_j^{(k)}=\sum_{m=-n+1}^{n} h_m^{(k)}e^{imj} \tag{11}$$

for $-n<j\leqslant n$. The latter is written in shortened notation as

$$a^{(k)}=\mathcal{F}[h^{(k)}], \tag{12}$$

where $\mathcal{F}$ denotes the Fourier transform, which will be chosen as the FFT algorithm, thus imposing that $n$ is an integer power of 2. The intermediate mapping $\omega^{(k)}$ is computed from the $a^{(k)}$ as

$$\omega_j^{(k)}=(i/n)a_j^{(k)} \quad \text{for} \quad j>0,$$
$$\omega_0^{(k)}=(i/2n)a_0^{(k)}, \tag{13}$$
$$\omega_j^{(k)}=0 \quad \text{for} \quad j<0.$$

The latter form is obtained from the identification of Eq. (8b) and the definition of $a^{(k)}$, taking care that one sum is over a positive index, while the other extends over the interval $[1-n,n]$. Then, one computes the series

$$b_j^{(k)}=ia_j^{(k)} \quad \text{for } j>0,$$
$$b_0^{(k)}=0, \tag{14}$$
$$b_j^{(k)}=\overline{b_{-j}^{(k)}}=-\overline{ia_{-j}^{(k)}}=-ia_j^{(k)} \quad \text{for} \quad j<0.$$

This linear transformation is written in shortened notation as

$$b^{(k)}=\mathcal{G}[a^{(k)}], \tag{15}$$

where $\mathcal{G}$ is the above detailed transformation. The form of $\mathcal{G}$ is dictated by Eq. (8a) for a positive index, and from the fact that the inverse Fourier transform of $b$ (see below) is real. The new sampling series is finally obtained from

$$u_j^{(k+1)}=\frac{j\pi}{n}+\mathcal{F}^{-1}[b^{(k)}]. \tag{16}$$

Equations (10)–(16) define one step in the algorithm relating $\omega^{(k+1)}$ to $\omega^{(k)}$. We give this shortened notation for this step as $\omega^{(k+1)}=\mathcal{T}(\omega^{(k)})$.

The searched function $\Omega$ is clearly a fixed point of the transformation $\mathcal{T}$ defined above in a discretized version. The uniqueness of the transformation $\Omega$ results from that of the harmonic field in the domain $\mathcal{E}$ with an equipotential condition on the boundary and a constant gradient perpendicular to the boundary at an infinite distance from it. Therefore, the only condition to consider is the stability of the fixed point.

### B. Stability

Let us assume that we have an approximate solution of the transformation $\Omega(z)$, from which we compute the series $u_j$. All intermediate quantities computed from the exact solution are denoted by a superscript $*$. Following one complete iteration of the algorithm, we obtain the following expressions:

$$u_j=u_j^*+\delta u_j,$$
$$h_j=h_j^*+h'(u_j^*)\,\delta u_j,$$
$$a=a^*+\mathcal{F}[h-h^*], \tag{17}$$
$$b=b^*+\mathcal{G}[a-a^*],$$
$$(\delta u)'=\mathcal{F}^{-1}[b-b^*],$$

where a Taylor expansion of $h$ has been used to estimate the values of $h-h^*$ and where indices are omitted when unnecessary. The resulting difference $(\delta u)'$ after one cycle is thus

$$(\delta u)'=\mathcal{F}^{-1}\mathcal{G}\mathcal{F}[h'(u_j^*)\,\delta u_j]. \tag{18}$$

Let us introduce the norm

$$\|u\|^2\equiv\sum_j |u_j|^2. \tag{19}$$

Parseval's theorem relates the above norm in real and Fourier spaces according to

$$\|\mathcal{F}(h)\|=\sqrt{2n}\|h\|. \tag{20}$$

In a similar fashion, the transformation $\mathcal{G}$ does not affect the norm:

$$\|\mathcal{G}(h)\|=\|h\|. \tag{21}$$

Using the two previous results, we can estimate the norm of $(\delta u)'$ as

$$\|(\delta u)'\|^2=\sum_j h'(u_j^*)^2(\delta u_j)^2\leqslant\max(|h'|)^2\|(\delta u)\|^2. \tag{22}$$

Therefore, if the absolute value of the slope of the objective profile satisfies

$$|h'(u)|<1 \tag{23}$$

for all $u$, then the fixed point $\Omega^*$ is attractive for the transformation $\mathcal{T}$. It should, however, be noted that the number of modes $n$ should be large enough so that the perturbation $\delta u$ should be small enough to legitimate the Taylor expansion of $h$ used in the stability analysis.

In practice, the convergence is very fast provided the sufficient condition (23) is fulfilled. Moreover it has to be noted that one step in the algorithm requires a rather limited amount of computing time of order $n\ \ln(n)$ (i.e., as for a FFT operation). Considering that this computation gives the solution of a harmonic problem in a semi-infinite domain, this cost appears to be extremely low.

When our algorithm is applied to a simple monochromatic sine (or cosine) profile, $h(u)=A\ \sin(u)$, it turns out that as soon as the condition (23) is violated (i.e., $A\geqslant 1$) the scheme is unstable, and a loop begins to appear around the origin where the slope exceeds 1. Thus the sufficient condition is also a necessary condition.

The limit $|h'(u)|<1$ can simply be broken if one uses an under-relaxation scheme. The optimum determination of the under-relaxation parameter, or the use of other algorithms can be found in Ref. [31] for mapping arbitrary domains on the unit disk. The transposition of these algorithms to our problem can be worked out in detail. Other ways to break this limit is to decompose the transformation $\Omega$ in two (or more) substeps. Suppose one could map the real axis onto an intermediate profile using a first transformation $\Omega_1$ and then the intermediate profile onto the objective one using a second transformation $\Omega_2$. The combination of the two transformations $\Omega(z)=\Omega_2(\Omega_1(z))$ is then the searched mapping. By breaking the problem into two steps, it is possible that each step can be handled by the above presented algorithm, while the combination of the two gives a profile having a slope

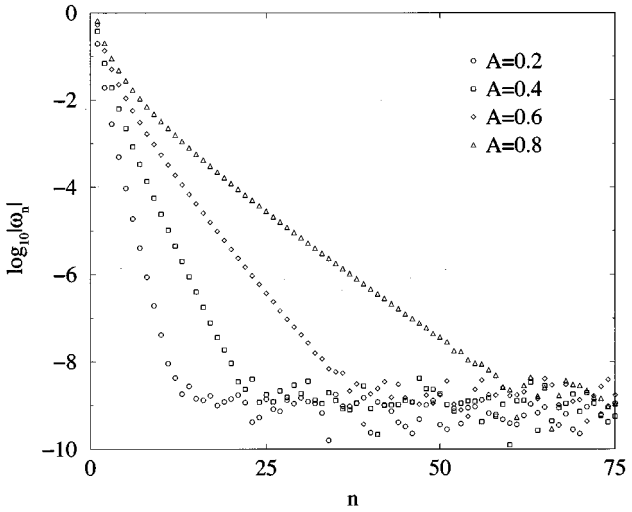


FIG. 3. Power spectrum of the function $\omega$ computed for a sine profile. The four curves correspond to four amplitudes, $A=0.2(\bigcirc)$, 0.4 ($\square$), 0.6 ($\diamond$), and 0.8 ($\triangle$).

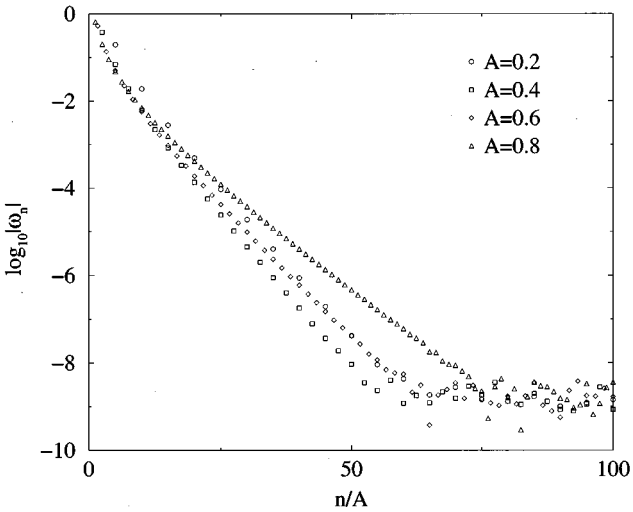


FIG. 4. Power spectrum of the function $\omega$ computed for a sine profile in the reduced coordinate $n/A$. The four curves correspond to four amplitudes, $A=0.2$ $\bigcirc$), 0.4 $\square$, 0.6 ($\diamond$), and 0.8 ($\triangle$). One observes a reasonable collapse for the three smallest amplitudes.

larger than unity. The difficulty here is to devise a suited intermediate step. One could consider, for example, filtering the initial objective profile so that the filtered profile may fulfill the slope constraint. We did not investigate this extension any further.

### C. Convergence and example application

We present in the following calculations of conformal transformations associated with a simple sine interface. We will use a norm on the error similar to the one introduced in Sec. III B. The distance $d$ between the objective profile and the calculated one is defined as follows:

$$d^2=\frac{1}{2\pi}\int_0^{2\pi}[h(u(x))-\Omega(x)]^2dx. \tag{24}$$

It is convenient to make this distance dimensionless, normalizing it by the amplitude of the profile, $d^*=(d/A)$, where the objective profile has the equation $h(u)=A\sin(u)$.

It is worth noting that the problem is far from being as simple as it might appear on the surface. In real space one single Fourier mode is sufficient to entirely characterize the interface. The transformation $\Omega$, however, requires many more modes. Figure 3 shows the power spectrum of the $\omega$ series for different amplitudes $A$. One can see that the contribution of the different modes decreases exponentially fast with the wave number $n$ but that the number of important modes increases roughly linearly with the amplitude of the sine profile. These observations suggested the scaling of the axis chosen in Fig. 4 for illustrating the above-mentioned rough trends.

The convergence of the algorithm is shown in Fig. 5, where the profiles obtained after the first few iterations are shown. In this particular example $A=0.5$ and the number of modes is 32.

The importance of allowing for enough Fourier modes is also illustrated by considering the minimum error $d$ obtained as a function of $n$ as shown in Fig. 6. (For this particular study we did not resort to a FFT algorithm to handle any value of $n$.) For $A=0.5$ we observe that about 20 modes are necessary to reach the single precision used in the computation. As the amplitude increases, the number of modes needed to reach a small enough error becomes larger and larger.

## IV. SELF-AFFINE BOUNDARIES

In the description of rough surfaces and interfaces, some recent progress has been achieved by recognizing some scaling invariance properties that have been observed in a number of real surfaces, and have been shown to result naturally in a number of growth models. Recent reviews [5–7] have covered this field.

Due to the different roles played by the directions normal and parallel to the surface, the scaling invariance—when applicable—involves different scale factors depending on

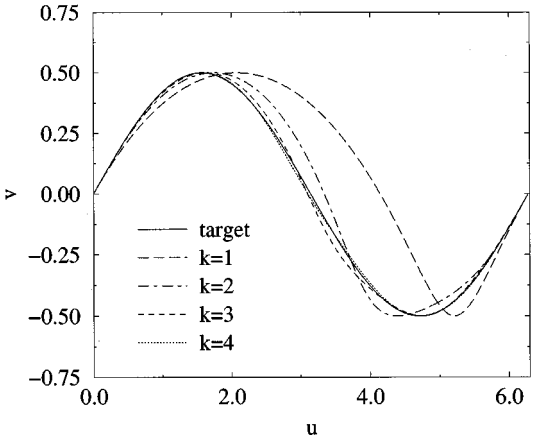


FIG. 5. Images of the real axis obtained after the first $k$ iterates of the algorithm with the objective profile $[h(u)=A\sin(u)]$ shown as a bold line. In this particular example $A=0.5$ and the number of modes is 32.

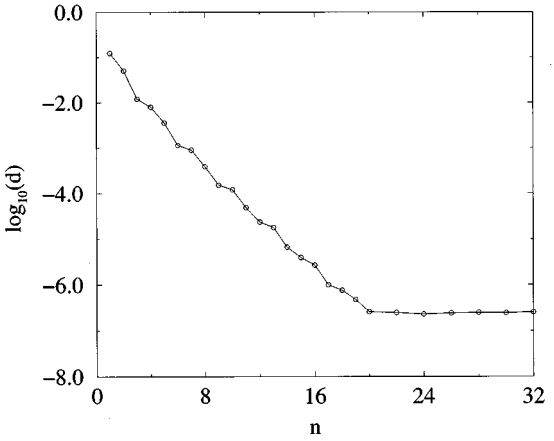


FIG. 6. Minimum error obtained using the algorithm described in the text for computing the conformal map on a sine profile with amplitude $A=0.5$, as a function of the number $n$ of modes used in $\omega$.

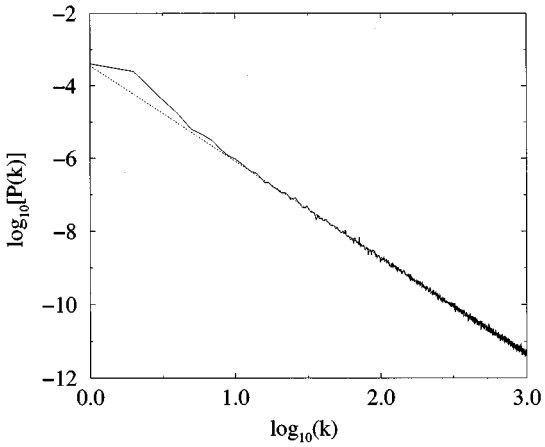


FIG. 7. Power spectrum of the image of the real axis obtained from synthetic transformation $\Omega$, obtained from Eq. (29). The roughness exponent used is $\zeta=0.8$. The best power-law regression on this power spectrum has a slope $s=-1.32$, which corresponds to an estimated roughness exponent $\zeta'=0.82$, equal within error bars to $\zeta$.

orientation, a property called self-affinity. We consider here only two-dimensional media so that the boundary is self-affine if it remains (statistically) invariant under the transformation

$$\begin{aligned} x &\to \lambda x, \\ y &\to \lambda^{\zeta} y \end{aligned} \tag{25}$$

for all values of $\lambda$. The exponent $\zeta$ is called the ''Hurst'' or roughness exponent. It is characteristic of the scaling invariance. From this property, we derive easily that

$$\langle [y(x)-y(x+\delta)]^2 \rangle = C^2 \delta^{2\zeta}, \tag{26}$$

where $C$ is a prefactor.

It is noteworthy that the self-affinity property does not involve the scaling of any measure. However, studying the scaling of the length of the curve, two regimes are revealed. For large distances, larger than a scale $\lambda$, the curvilinear length of the profile is simply proportional to the projected length along the $x$ axis, hence one can identify a trivial fractal dimension equal to 1. On the other hand, for distances smaller than $\lambda$, the arc length scales in a nontrivial fashion with the projected length. This allows one to define a fractal dimension equal to $d_f=2-\zeta$. The crossover scale $\lambda$ between these two regimes is such that the typical slope of the profile is 1, i.e., using the notations of Eq. (26),

$$\lambda = C^{1(1-\zeta)}. \tag{27}$$

Once a roughness profile has been measured, a very convenient way [32] to check the self-affinity is to compute the power spectral density (PSD) of the profile. In the case of a self-affine profile of exponent $\zeta$, the PSD is expected to have the following behavior:

$$P(k) \propto k^{-1-2\zeta}. \tag{28}$$

It is important to stress that the approach developed in this paper is not specific to self-affine boundaries. However, being given the practical importance of such boundaries, and the expected generality of scaling results, we will essentially focus on self-affine boundaries as practical applications of the concepts developed in the framework of the harmonic field in the vicinity of rough boundaries.

In view of the form of the transformation $\Omega$, and of the previous scaling, Eq. (28), we introduce a particular set of transformation: let us choose

$$\omega_k = A \epsilon_k k^{-1/2-\zeta}, \tag{29}$$

where $\epsilon_k$ is a random Gaussian variable with zero mean and unit variance for the real and imaginary parts independently; we can write

$$\mathrm{Re}\left[\frac{\partial \Omega}{\partial x}(x+i0)\right] = 1 + A\ \mathrm{Im}\left[\sum_k \epsilon_k k^{1/2-\zeta} e^{-ikx}\right]. \tag{30}$$

Then for a given set of $\epsilon_k$, we can define a maximum amplitude such that the mapping is bijective:

$$A_{\max} = \frac{-1}{\mathrm{Im}[\Sigma_k \epsilon_k k^{1/2-\zeta} e^{-ikx}]}. \tag{31}$$

This method gives a short way to generate directly $\Omega$ transforms, which image the real axis to a self-affine interface shape. This approach is useful to study generic properties of self-affine boundaries.

When the amplitude $A$ is small enough, $u \approx x$, and thus the series $\omega_k$ is equal to the Fourier transform of the profile. The transformation $\Omega$ sends the real axis onto a periodic function whose power spectrum is of the form Eq. (28). When the amplitude increases, the first iteration of the algorithm turns out to be rather approximative. In order to show that the power spectrum of $\omega_k$ is not significantly altered by further steps, we show in Fig. 7 the power spectrum of $\omega_k$ as compared to the initial zeroth-order approximation. The results have been obtained from an average over 100 profiles

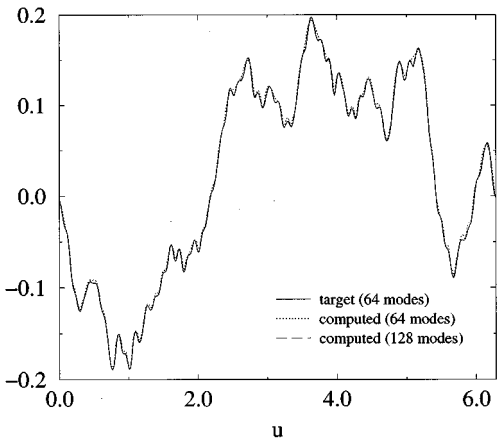


FIG. 8. An example of the obtained profile $\partial\mathcal{E}$ from the conformal map, compared to the objective one, chosen to be a self-affine function with a roughness exponent $\zeta=0.8$. The amplitude of the profile is 95% of the maximum amplitude, which preserves the convergence of the algorithm.

with 2048 modes each. We see that the synthetic generation of the transform does not modify the power spectrum of $\omega$ coefficients.

Therefore, we can directly generate mappings $\omega$ that will transform the real axis into a periodic boundary that is self-affine with any prescribed roughness exponent for distances smaller than the period. Such a construction may appear as artificial in the sense that the rough boundary is not imposed but, on the contrary, it results from the choice of the mapping. It is, however, useful, as will be shown later, because it allows one to study generic properties of harmonic fields close to self-affine boundaries.

The alternative way consists in using the mapping construction algorithm. As mentioned above, we have analyzed the convergence of the algorithm applied to the special case of a sine profile. We now consider the case of a self-affine boundary in a similar fashion. This interface has been calculated in the real space with 64 modes, and we have used 256 modes in the conformal transformation. The standard deviation of the height distribution is called $\sigma$. The chosen $\zeta$ exponent chosen for this example is $\zeta=0.8$. From Eq. (31), we note that the maximum amplitude decreases as the number of modes $n$ increases. This is natural since as the lower cutoff in the scaling regime decreases, the self-affine function will tend toward a continuous but nondifferentiable curve when $0<\zeta<1$. The distribution of local slopes is indeed expected to get wider and wider as the number of modes increases. Quantitatively, $A_{\max}\propto n^{\zeta-1}$. It is to be noted that as $n$ increases, the standard deviation of the height $\sigma$ does not increase. It is to be noted that these conclusions are drawn under the hypothesis that the longest wavelength remains fixed; here it is set to $2\pi$. Alternatively, if the smaller cutoff and the amplitude of the corresponding mode were kept constant while increasing the number of modes, then the maximum amplitude would remain constant.

As in the previous example (sine profile), we can observe in Fig. 8 an example of the conformal map obtained for $\sigma/\sigma_{\max}=0.95$, where the maximum standard deviation that could be handled by the algorithm without diverging is $\sigma_{\max}\approx 0.1$. We can see in this figure that the major differences between the objective and calculated profiles occur in areas where the local slope is maximum. For roughness amplitude greater than the convergence threshold, one can see loops appearing in these areas. The convergence speed, the sensitivity to the number of modes allowed in the determination of $\Omega$, the evolution of the minimum error, etc. behaved for these self-affine profiles in a similar qualitative way as for the simple sine profile.

## V. GENERIC PROPERTIES OF HARMONIC POTENTIALS

In the following, we show that the knowledge of such a conformal transformation allows one to solve immediately harmonic problems. We essentially focus here on the case where the field is assumed to be uniform far from the boundary. This is a typical case as soon as the roughness is of small amplitude. This can be seen as an asymptotic expansion focusing here on the small scale details of the interface, whereas the matching with the far field can be done using a field whose variation is small on the scale of the roughness amplitude. We will now focus on two problems: a perfectly conducting boundary so that the potential gradient is normal to the boundary, and a perfectly insulating boundary where the potential gradient is parallel to the surface. Since we know how to tailor mappings that image the real axis on a generic self-affine boundary, this gives us an opportunity to consider the scaling features of harmonic fields in the vicinity of self-affine boundaries.

Harmonic fields are encountered very frequently in nature. Linear transport involving scalar fields $\Phi$, where the flux $J$ is proportional to the field gradient plus a conservation law in the absence of sources and, under steady conditions $\mathrm{div}(J)=0$, implies the harmonic nature of the field $\Phi$, $\nabla^2\Phi=0$. Heat diffusion obeying Fourier's law gives a harmonic temperature field under steady conditions. Mass diffusion with Fick's law is a similar example with the concentration field. Electric conduction with Ohm's law, viscous flow in confined two-dimensional Hele-Shaw cells, vorticity in Stokes flow, etc. constitutes a partial list of possible applications.

### A. Homogeneous far field

In this part, for the sake of concreteness, we use the case of thermal conduction. We are interested in the temperature field $T$ in the region $\mathcal{E}$ limited by the rough interface $\partial\mathcal{E}$. Let us first consider the case of a perfectly conducting interface, so that $T=T_0$ for each point of the boundary. We impose in the far field a homogeneous unit flux of heat. The problem to solve is

$$\nabla_w^2 T=0 \quad \text{in} \quad \mathcal{E},$$
$$T=T_0 \quad \text{on} \quad \partial\mathcal{E}, \tag{32}$$
$$\vec{\nabla}T(w)\to\vec{e}_v \quad \text{if} \quad v\to-\infty.$$

The knowledge of $\Omega$ allows one to define $\Theta$, the image field of $T$ in the smooth domain $\mathcal{D}$: $\Theta(z)=T\circ\Omega(z)=T(w)$. As $\nabla_z^2\Theta=\nabla_w^2 T|\Omega'(z)|^2$ and $\Omega'(z)\neq 0$ in $\mathcal{D}$, the resolution of Eq. (32) in $\mathcal{E}$ is thus equivalent to

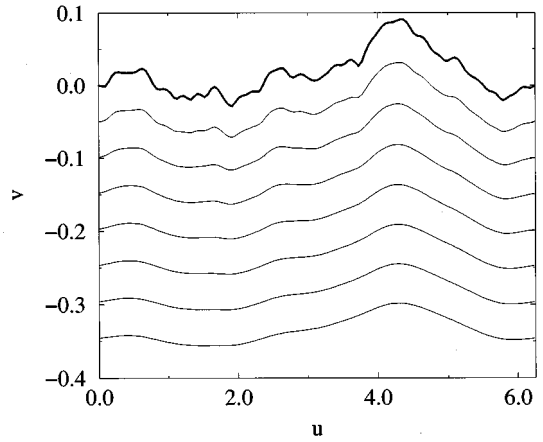


FIG. 9. Example of isotherm curves close to a rough self-affine boundary on which the temperature is constant, whereas the temperature gradient is homogeneous and vertical far from the boundary.

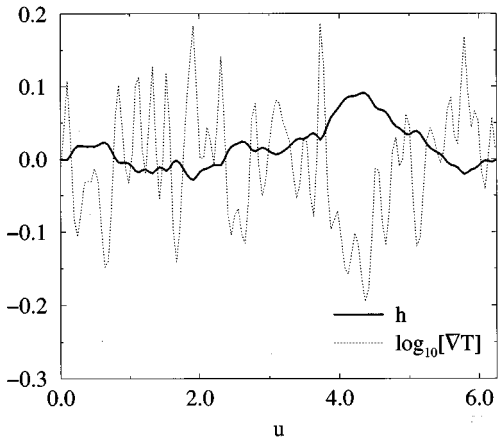


FIG. 10. Profile $h(u)$ of the rough boundary (bold line) and temperature gradient $\partial_n T(u)$ (dotted line) on the surface of the same boundary. We note strong correlations between the two curves.

$$\nabla_z^2 \Theta(z) = 0 \quad \text{in} \quad \mathcal{D},$$
$$\Theta(z) = T_0 \quad \text{on} \quad \partial\mathcal{D}, \tag{33}$$
$$\vec{\nabla}\Theta(z) \to \vec{e}_y \quad \text{if} \quad y \to -\infty.$$

The frontier $\partial\mathcal{D}$ being the real axis, we have immediately the solution in $\mathcal{D}$: $\Theta(z) = T_0 + y$ and then the solution in $\mathcal{E}$ is

$$T(w) = T_0 + \mathrm{Im}[\Omega^{-1}(w)]. \tag{34}$$

Figure 9 shows a set of isotherm curves close to a self-affine isotherm boundary. These lines become smoother and smoother when the distance to the electrode increases. The morphology of these isotherm lines has some interesting features. If $\Delta$ denotes the distance from the boundary, one can observe from the form of the mapping $\Omega$ that modes with a wavelength smaller than $\Delta$ will be damped whereas longer wavelength modes will only be slightly decreased. Therefore, the isotherm curves will be similar to the profile up to a low pass filtering. In the case of a self-affine boundary, the isotherms will preserve the self-affine character with the same exponent, but their lower cutoff will increase as the distance to the actual boundary, up to the distance of order of the largest wavelength.

Let us now study the temperature gradient. Quite generally, we can write the gradient in the complex plane as

$$\nabla_w T(w) \equiv (\partial_u + i\partial_v) T(w) = 2\partial_{\bar{w}} T. \tag{35}$$

From the expression of the temperature field, we have

$$\nabla_w T(w) = i\overline{\Omega^{-1\prime}(w)} = i[1 + \overline{\omega'(z)}]^{-1}. \tag{36}$$

From the expression of the function $\omega$, we see that at a large distance from the rough boundary, the term $\omega'$ vanishes exponentially. Therefore, one recovers the imposed condition for the temperature at infinity, i.e., $\nabla T \to i$.

In Figure 10 we have presented both the profile of a rough electrode and the modulus of the temperature gradient. One may see quite easily that the field is very large (small) in the deepest (highest) areas. This field depends naturally both on the local topography and on its remote environment. The connection between the field and the local topography can be analyzed through cross correlations, as will be done below.

The perfectly insulating boundary is the other archetypical problem whose expression is

$$\nabla_w^2 T = 0 \quad \text{in} \quad \mathcal{E},$$
$$\partial_n T = 0 \quad \text{on} \quad \partial\mathcal{E}, \tag{37}$$
$$T(w) \to u \quad \text{if} \quad v \to -\infty.$$

The solution to this problem can simply be obtained from the previous solution using duality properties of the harmonic field. The real part of the previous solution gives the answer to the problem:

$$T(w) = \mathrm{Re}[\Omega^{-1}(w)]. \tag{38}$$

The temperature gradient is then simply

$$\nabla_w T(w) = [1 + \overline{\omega'(z)}]^{-1}. \tag{39}$$

### B. ''Equivalent'' smooth boundary condition

We have seen previously that once we know the conformal mapping capable of transplanting the half complex plane $D$ onto the rough domain $E$, we have immediately the solution of the electrical potential near the rough electrode $\partial E$. If the roughness amplitude remains below the convergence threshold, we will be able to solve this problem for any kind of boundary. In practice, very often, one does not worry about the details of the rough interface. As we have seen most perturbations die away from the boundary exponentially fast. Therefore, knowing the longest wavelength of the boundary gives the scale away from the boundary where the field becomes homogeneous.

This means, practically, that if one is interested only in the far field, one could replace the rough interface by a straight one so that the far field is unperturbed. The question we want to address in this section is the following: where should the ''equivalent'' straight interface be located so as to

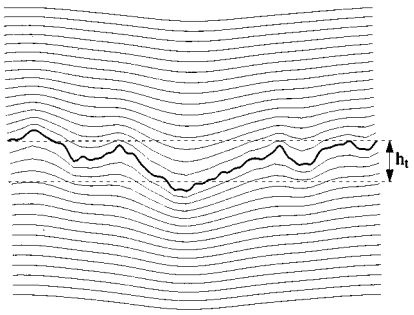


FIG. 11. Schematic illustration of the finite ''electrical'' thickness of a rough equipotential. The rough equipotential $C$ (shown as a bold curve) is placed in between two remote planar electrodes. The presence of the rough equipotential reduces the resistance of the medium in a similar way as an planar equipotential with a finite thickness. Extrapolating the far electrical field from the remote electrodes gives ''equivalent'' smooth boundaries shown as dotted lines. Their relative distance defines the ''electrical'' thickness $h_t$.

match the asymptotic far field? A zeroth-order guess is to place it at the geometrical average of the height distribution. This will be shown to be not to an exact answer; in the following, we call $H$ the distance between the equivalent position and the geometrical average.

In order to illustrate the problem, let us imagine the following experiment. Let us consider an electrolytic bath, where the electrical field is homogeneous between two opposite electrodes $A$ and $B$ at a distance $L$ from each other. The electrical resistance $R$ of the set-up is measured. Then, as illustrated in Fig. 11 we place in the middle of the bath and parallel to the electrodes a rough plane $C$ of negligible thickness that is a good conductor, so that it can be considered as an equipotential. We measure again the electrical resistance of the setup, which is now reduced to $R-\Delta R$. What is the value of $\Delta R$? To answer this question, we divide the system in two, $A$-$C$ and $B$-$C$. Each of these two problems corresponds to the situation described in the introduction of this section. Extrapolating the field from electrode $A$, we find an offset $H_1$. Similarly, from $B$ we obtain a different offset $H_2$, so that, ignoring the details of the perturbed field in the vicinity of $C$, the rough electrode will appear to be equivalent to a plane electrode of thickness $H_t = H_1 + H_2$. This ''electrical thickness'' has nothing to do with the real thickness of the plane considered here to be zero. If the rough electrode has the shape of a sine function, of amplitude $A$ and wavelength $\lambda$, we will argue below that $H_t \propto A^2/\lambda$. Finally it is a simple matter to relate the resistance drop to this effective thickness through $\Delta R/R = H_t/L$.

We now revert to the notation of the previous paragraph, and deal with the temperature instead of the voltage. For distances away from the rough boundary much greater than $2\pi$ (our longest wavelength), all exponential terms die out, and hence the far field can be written as

$$T(w) \approx T_0 + \mathrm{Im}(w - \omega_0), \tag{40}$$

where $\omega_0$ is the constant term in the function $\omega$. The offset position of the equivalent isotherm is thus

$$H = \mathrm{Im}(\omega_0). \tag{41}$$

Let us first analyze the problem for a small amplitude sine boundary of amplitude $A$ and wavelength $\lambda$. The offset $H$ in the location of the equivalent straight boundary is to be normalized by $A$ to obtain a dimensionless quantity. The latter should be a function of the dimensionless ratio $A/\lambda$. Taylor expansion of this function provides the perturbation expansion

$$H = a_0 A + a_1 \frac{A^2}{\lambda} + a_2 \frac{A^3}{\lambda^2} + O(A^4/\lambda^3). \tag{42}$$

A simple argument allows one to simplify the latter equation. Suppose one would analyze the problem for the profile of amplitude $-A$. The latter is obtained from the former by a translation along the $x$ axis by an amount $\lambda/2$. Thus $H$ should be unchanged. This imposes that odd terms in the expansion should vanish, hence,

$$H = a_1 \frac{A^2}{\lambda} + O(A^4/\lambda^3). \tag{43}$$

Thus the dominant correction is of order $A^2/\lambda$. It can be interpreted as the product of the amplitude $A$ and a typical slope $(A/\lambda)$. This result holds in the limit of a small amplitude and long wavelength. If the wavelength goes to zero, clearly the offset should converge to the amplitude, but the latter limit cannot be obtained from the above Taylor expansion in the small parameter $A/\lambda$.

For a sine profile of small amplitude it is possible to carry out the computation of the coefficient $a_1$. We briefly sketch here the solution. The potential is to be computed to second order in $A$. We revert, as above, to a wavelength $\lambda = 2\pi$. The solution reads

$$T(w) = T_0 + \mathrm{Im}[w + (i/2)A^2 - Ae^{-iw} - (i/2)A^2 e^{-2iw}] + O(A^3). \tag{44}$$

The offset can be read from this equation as $H = (1/2)A^2$. Reincorporating the $\lambda$ dependence, we arrive at $a_1 = \pi$ or

$$H = -\pi \frac{A^2}{\lambda} + O(A^4/\lambda^3). \tag{45}$$

This last result is of course only valid for small $A$ values, $H$ being bounded by $A$. In Figs. 12 and 13, we can see comparisons between this perturbative calculation and the result directly obtained by conformal transformation. We observe excellent agreement for small amplitudes (large wavelengths) and then the perturbative calculation overestimates $H$ for larger values of the amplitude (smaller wavelength). In view of the upper bound on the offset and the above perturbation expansion, we propose the following form:

$$H \approx -\frac{2A}{\pi} \arctan\left(\frac{\pi^2 A}{2\lambda}\right), \tag{46}$$

which fits the data accurately as can be seen on Figs. 12 and 13, and which reproduces both limiting behaviors $\lambda \to 0$ and $\lambda \to \infty$.

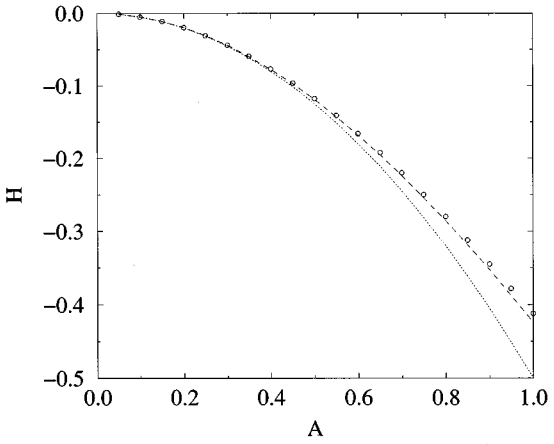


FIG. 12. Offset $H$ of the equivalent boundary from the geometrical average of a sine profile of variable amplitude $A$ and fixed wavelength $\lambda=2\pi$. The dotted line is the result of the perturbation analysis, Eq. (43) and the symbols are the results obtained from a conformal mapping. The dashed curve is the proposed fit Eq. (46).

We now ask how the result translates to a rough profile. In particular for a self-affine profile, there is no characteristic length scale apart from the cutoffs. The product of the amplitude times the slope is a scale-dependent factor. Is it possible to reach quantitative conclusions for such profiles?

In order to estimate $H$ for a rough boundary, we use the formalism developed for introducing the algorithm. We expand the function $\omega$ as well as all other intermediate quantities in the series of the profile amplitude. Using the linearity of the transformations $\mathcal{F}$, $\mathcal{G}$, and $\mathcal{F}^{(-1)}$, we arrive at

$$H=\mathrm{Im}[\omega_0]=\frac{\mathrm{Re}[a_0]}{2n}=\frac{1}{2n}\sum_j h_j^* =\frac{1}{2n}\sum_j h'(u_j)\mathcal{F}^{(-1)}\circ\mathcal{G}\circ\mathcal{F}[h_j] \tag{47}$$

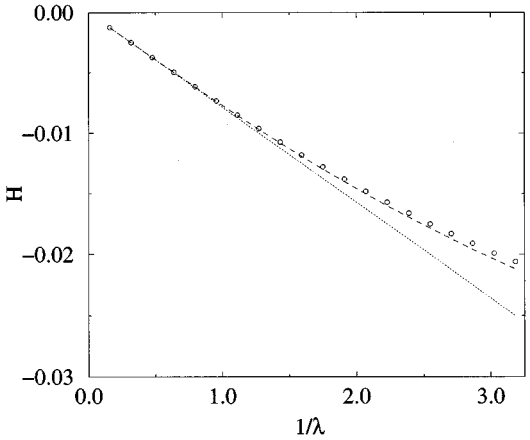


FIG. 13. Offset $H$ of the equivalent boundary from the geometrical average of a sine profile of amplitude $A=0.05$ and variable wavelength $\lambda$. The dotted line is the result of the perturbation analysis [Eq. (43)] and the symbols are the results obtained from a conformal mapping. The dashed curve is the proposal fit, Eq. (46).

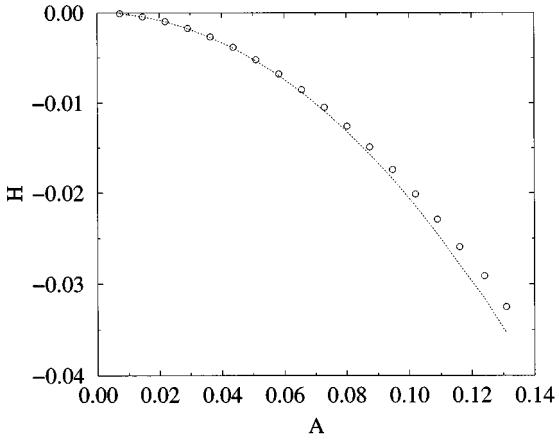


FIG. 14. Offset $H$ of the equivalent boundary from the geometrical average of a self-affine profile of variable amplitude $A$, a roughness exponent $\zeta=0.8$ and 16 modes. The dotted line is the result of the perturbation analysis [Eq. (49)] and the symbols are the results obtained from a conformal mapping.

up to third-order terms in the amplitude. We now need an asymmetric version of Parseval's theorem. Let us compute the integral for two arbitrary arrays defined in real space for $u$ and Fourier space for $v$:

$$\sum_j u_j\mathcal{F}^{(-1)}[v]_j=\frac{1}{2n}\sum_j\sum_k u_j v_k e^{-ikj}=\frac{1}{2n}\sum_k \overline{\mathcal{F}[u]_k}v_k. \tag{48}$$

The offset can now be expressed as

$$\begin{aligned} H&=\frac{i}{4n^2}\sum_k \overline{\mathcal{F}[h]_k}\mathcal{G}\circ\mathcal{F}[h(x)]_k k \\ &=-\frac{1}{4n^2}\left(\sum_{k>0}\tilde{h}_k\overline{\tilde{h}_k}k-\sum_{k<0}\overline{\tilde{h}_k}\tilde{h}_k k\right) \\ &=-\frac{1}{2n^2}\sum_{k>0}|\tilde{h}(k)|^2 k, \end{aligned} \tag{49}$$

where $\tilde{h}_k$ is the Fourier transform of $h_j$.

Figure 14 gives the evolution of $H$ with the amplitude of self-affine profiles of roughness exponent $\zeta=0.8$, and 16 modes. Again, we observe that the expression (49) is accurate for small amplitude, but shows deviations for larger amplitudes.

It is interesting to consider the scaling of $H$ observed from the generic transformations where $\omega_k$ are postulated to be $\omega_k=A\epsilon_k k^{-1/2-\zeta}$. The expectation value of the offset $\langle H\rangle$ reads, to dominant order in the amplitude,

$$\langle H\rangle=A^2\sum_{j=1}^{n} j^{-2\zeta} \tag{50}$$

where the extra factor of 2 comes from the expectation value of $\langle|\epsilon|^2\rangle=2$, since real and imaginary parts of $\epsilon_k$ are independent Gaussian variables of zero mean and unit variance. Depending on the value of the roughness exponent $\zeta$ two cases are to be distinguished.

(1) For a ''*persistent*'' profile—i.e., $\zeta>0.5$—the sum in Eq. (50) is dominated by the smallest $j$, i.e., the longest wavelength, and thus the scaling of $\langle H\rangle$ can be expressed as

$$\langle H\rangle = Z(2\zeta)\,\frac{A^2}{4}\left(\frac{2\pi}{\lambda_{\max}}\right)^{-2\zeta}, \tag{51}$$

where $Z(s)=\Sigma_1^\infty k^{-s}$ is the Riemann zeta function. We have dropped momentarily the convention that the largest wavelength is $2\pi$; hence $\lambda_{\min}$ and $\lambda_{\max}$ are respectively the smallest and largest cutoff lengths in the profile. In this case, $A$, the amplitude, is such that the largest wavelength mode amounts to $A\epsilon_1(2\pi/\lambda_{\max})^{-1/2-\zeta}$. Let us introduce the standard deviation of the profile given by

$$\sigma^2=\frac{1}{\lambda_{\max}}\int h(x)^2dx=\frac{1}{2n}\sum_j h_j^2, \tag{52}$$

which leads (using Parseval's theorem) to

$$\langle\sigma^2\rangle=\frac{1}{4n^2}\sum_k |\tilde{h}_k|^2=Z(2\zeta+1)\,\frac{A^2}{2}\left(\frac{2\pi}{\lambda_{\max}}\right)^{-2\zeta-1} \tag{53}$$

with $\zeta$ similar to the scaling Eq. (26).

Equation (50) can then be expressed as

$$\langle H\rangle=\pi\,\frac{Z(2\zeta)}{Z(2\zeta+1)}\,\frac{\langle\sigma^2\rangle}{\lambda_{\max}}. \tag{54}$$

The latter equation simply means that the rough profile behaves as a simple monochromatic profile. This conclusion is, however, not always valid, as is shown in the following case.

(2) For an ''*antipersistent*'' profile—i.e., $\zeta<0.5$—the sum in Eq. (50) is dominated by the largest $j$, i.e., the shortest wavelength, in contrast to the previous persistent case,

$$\langle H\rangle\propto A^2\lambda_{\max}^{2\zeta}\left(\frac{\lambda_{\min}}{\lambda_{\max}}\right)^{2\zeta-1}. \tag{55}$$

Therefore, we can express the scaling of $H$ in an intrinsic fashion as

$$\langle H\rangle\propto\frac{\langle\sigma^2\rangle}{\lambda_{\max}}\left(\frac{\lambda_{\min}}{\lambda_{\max}}\right)^{2\zeta-1}. \tag{56}$$

In contrast to the persistent case, it appears that the offset $H$ is dependent on the lower cutoff scale of the profile. In fact if $\lambda_{\min}$ is kept fixed, the standard deviation $\sigma$ grows as $\lambda_{\max}^{2\zeta}$. Therefore, one sees that the upper scale cutoff disappears, so that $H$ only depends on $\lambda_{\min}$. In order to see this more clearly, we introduce another measure of the roughness that is sensitive to the small scale. Let $\zeta$ be the norm of the derivative of $h$:

$$\zeta^2=(1/\lambda_{\max})\int h'(u)^2du=(1/2n)\sum_j h'(u_j)^2, \tag{57}$$

which amounts to

$$\langle\zeta^2\rangle\propto A^2\lambda_{\max}^{2\zeta-1}\left(\frac{\lambda_{\min}}{\lambda_{\max}}\right)^{2\zeta-2}. \tag{58}$$

From the latter norm, the offset can be written as

$$\langle H\rangle\propto\langle\zeta^2\rangle\lambda_{\min}, \tag{59}$$

which is the counterpart of Eq. (54) for the antipersistent case.

As a conclusion, the scaling of the offset $H$ is controlled by the shortest (longest) scale cutoff of the self-affine regime for antipersistent (persistent) boundaries.

### C. Correlation between local field and topography

Above, we extracted the expression of the temperature gradient as a function of the transformation $\omega$. We now use it to investigate the correlations between the topography and the temperature gradient. We study these correlations in the limit of small amplitude.

The first-order perturbation in the temperature gradient can be extracted from Eq. (36) as

$$|\nabla T|^2=1-\omega'(x)-\overline{\omega'(x)}+O(\epsilon^2), \tag{60}$$

where the amplitude of the profile is assumed to be of order $\epsilon$. We introduce the logarithm of the temperature gradient denoted by $\varphi$, which can be expressed as

$$\varphi\equiv\ln(|\nabla T|^2)=-2\,\mathrm{Re}[\omega'(x)]+O(\epsilon^2). \tag{61}$$

From now on we will omit the $O(\epsilon^2)$ term, keeping in mind that we focus here only on the dominant term.

In order to compute the correlation between the gradient of temperature and the height, we form the cross product and average over $u$ (or $x$ for convenience, since their difference is of order $\epsilon$). The expectation value of the product is

$$\langle\varphi(u)h(u)\rangle=-2\langle\mathrm{Re}[\omega'(x)]\mathrm{Im}[\omega(x)]\rangle=-2\sum_k k|\omega_k|^2. \tag{62}$$

It is amazing that the same expression appeared when computing the offset of the equivalent straight boundary.

We define now the correlation coefficient $\alpha$, which can be identified as the slope of a linear regression between $h$ and $\varphi$. Its value is

$$\alpha\equiv\frac{\langle\varphi(u)h(u)\rangle}{\langle h^2(u)\rangle} \tag{63}$$

since $\langle h\rangle=\langle\varphi\rangle=0$ to first order in $\epsilon$. Hence we have

$$\alpha=-2\,\frac{\Sigma_k k|\omega_k|^2}{\Sigma_k|\omega_k|^2}. \tag{64}$$

This expression holds for any rough boundary of small amplitude.

In the particular case of a self-affine boundary, we assume as above that the transformation $\omega$ can be taken as the one generated artificially from its Fourier decomposition. The latter expression can thus be written as

$$\alpha=-2\,\frac{\Sigma_k k^{-2\zeta}}{\Sigma_k k^{-1-2\zeta}}. \tag{65}$$

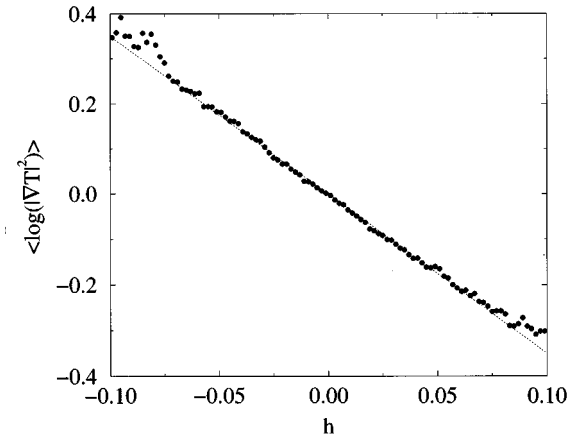


FIG. 15. Average of the logarithm of the temperature gradient $\langle\varphi\rangle=\langle\log_{10}(|\nabla T|^2)\rangle$, for fixed height $h$, as a function of $h$. The data points (● symbols) are averages over 1000 profiles of small amplitude, with a roughness exponent $\zeta=0.8$, and 64 Fourier modes. The theoretical prediction is shown as a dotted line of slope $\alpha^*$.

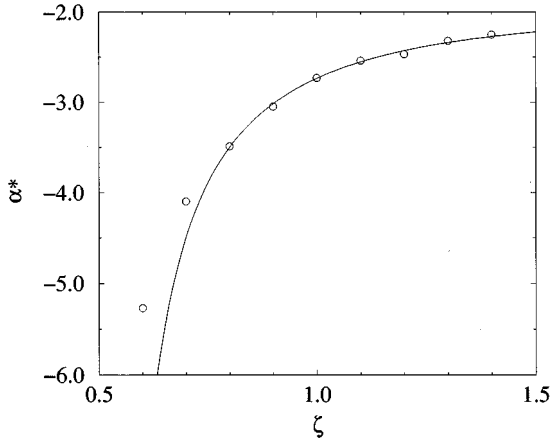


FIG. 16. Evolution of the limit $\alpha^*$ as a function of the roughness exponent $\zeta$. As $\zeta$ approaches 1/2, the coefficient diverges as $(\zeta-1/2)^{-1}$. The dotted line shows the predicted behavior and the symbols are the results computed from conformal mappings.

From the latter expression, we have to distinguish between persistent ($\zeta>1/2$) and anti-persistent ($\zeta<1/2$) profiles depending on whether the series is convergent or divergent when the number of modes increases.

In the case of a *persistent* self-affine boundary, as the number of modes increases to infinity, the value of $\alpha$ converges toward an asymptotic limit $\alpha^*$ given by a ratio of Riemann zeta functions:

$$\alpha^*=-2\frac{Z(2\zeta)}{Z(1+2\zeta)}. \tag{66}$$

The divergence of the zeta function as its argument approaches 1 leads to a divergence of $\alpha^*$ as $(\zeta-1/2)^{-1}$. In the more general case where $\lambda_{\max}$ is not set to $2\pi$, the above equation should be corrected to

$$\alpha^*=-2\frac{Z(2\zeta)}{Z(1+2\zeta)}\left(\frac{2\pi}{\lambda_{\max}}\right). \tag{67}$$

As a practical illustration of the latter property we have studied the correlations between $h$ and $\varphi$ by averaging $\langle\varphi\rangle$ at fixed $h$ for 1000 profiles having the same characteristics: amplitude $A=0.25A_{\max}$, roughness exponent $\zeta=0.8$, and 64 Fourier modes. Figure 15 shows the evolution of $\varphi$ versus $h$. From Eq. (66) we estimate $\alpha^*=-2Z(1.6)/Z(2.6)\approx-3.50$. As shown on Fig. 15, this value of $\alpha^*$ provides an accurate fit to the data. The evolution of this coefficient as a function of $\zeta$ is shown in Fig. 16.

The antipersistent self-affine profile behaves differently from the previous case. The correlation between the surface temperature gradient and the height vanishes. Mathematically, this result can be traced to the difference in behavior of the two series in Eq. (65). However, as in the previous section concerning the location of the equivalent smooth interface, one can extract the asymptotic behavior of $\alpha$:

$$\alpha=\frac{\langle\varphi(u)h(u)\rangle}{\langle h'^2(u)\rangle}\frac{\langle h'(u)^2\rangle}{\langle h(u)^2\rangle}=-2\left(\frac{2-2\zeta}{1-2\zeta}\right)\left(\frac{\lambda_{\min}}{2\pi}\right)\left(\frac{\zeta^2}{\sigma^2}\right). \tag{68}$$

This latter result sheds some light on the physical meaning of the previously mentioned divergence. In our presentation, we have chosen to fix the largest wavelength (set to $\lambda_{\max}=2\pi$) and amplitude of this mode. Increasing the number of modes implies that the shortest wavelength $\lambda_{\min}$ decreases. For roughness exponents in the range $0<\zeta<1$, this implies an algebraic increase of $\varsigma^2$ with $n$, while $\sigma^2$ is bounded. This divergence of $\varsigma^2$ is of no importance for the correlation $\alpha$ only if the profile is persistent. Otherwise, Eq. (68) holds. The perturbation method used, however, assumes that both $\sigma^2$ and $\varsigma^2$ should be small. The above analysis simply identifies which cutoff will dictate its behavior to the correlation. The antipersistent case is more suited to the case where $\lambda_{\min}$ is fixed together with its amplitude, while $\lambda_{\max}$ varies. In this case, the $\alpha$ coefficient increases as $\lambda_{\max}^{1-2\alpha}$ as can be read from Eq. (68) using the scaling $\sigma_2\propto\lambda_{\max}^{2\varsigma}$ ($\varsigma$ being independent of $\lambda_{\max}$.)

### D. Green function for harmonic problems on a rough interface

Up to now, we have only considered harmonic problems with a uniform field at infinity. This kind of boundary condition is of particular interest for problems where the scale of variation of the field in the bulk of the solid is large compared to the scale of the roughness so that an asymptotic development can be performed where the matching is to be done on the far field as one focuses on the rough boundary. However, from the conformal mapping, one can address more complex types of boundary conditions.

In order to illustrate this, we develop here a particular class of solutions that can be used to solve any problem. We will consider Green functions that give the field in the medium for localized flux $f$ injected in the medium from the surface.

Let us consider the following problem: a localized flux $f=1$ is injected at point (1,0), on the border of the unit circle $\mathcal{C}$. The remaining boundary is perfectly insulating. The same flux is withdrawn at the origin where $f=-1$. The harmonic field that fulfills such boundary conditions is

$$\Phi(z) = -\mathrm{Re}\left[\ln\left(\frac{(z-1)^2}{z}\right)\right]. \tag{69}$$

This potential $\Phi$ is the Green function for the domain $\mathcal{C}$. Considering the transformation $z \rightarrow -i\ln(z)$ maps the unit circle to the semiplane $\mathcal{D}$. In the transformation, the potential $\Phi$ becomes

$$\Phi(z) = -\mathrm{Re}[iz + 2\ln(1-e^{iz})], \tag{70}$$

which is the Green function for a unit flux localized at every site $(2k\pi,0)$ for all integers $k$. At infinity, the potential approaches $\Phi(z) \rightarrow y$. From this Green function it is simple to derive the one obtained for a translated array of sources. For sources at $(x_0 + 2k\pi,0)$, we have

$$\Phi(z,x_0) = -\mathrm{Re}[iz + 2\log(1-e^{i(x_0-z)})]. \tag{71}$$

From this latter expression, the Green function for a localized and periodic source on the rough profile is obtained by combining $\Phi$ and $\Omega$. The Green function thus reads

$$\Psi(w,w_0) = \Phi(\Omega^{-1}(w), \Omega^{-1}(w_0)), \tag{72}$$

which gives the potential at point $w$ for a series of sources periodically spaced with the same period as the profile $w_0 + 2k\pi$.

## VI. CONCLUSION

We have introduced here a conformal mapping technique that allows one to address harmonic problems in semi-infinite domains limited by a rough interface. This mapping is accompanied by an efficient numerical technique that allows us to compute the mapping by a few iterations of a one-dimensional Fourier transform. Moreover, this technique provides a natural basis for discussing analytically some practical applications.

We then defined and studied the notion of an equivalent smooth boundary, whose position has been obtained exactly in the limit of a small amplitude. This question underlined the differences between persistent and antipersistent boundaries, in terms of sensitivity to the lower or upper scale cutoff of the self-affine character of the boundary.

We considered the question of correlations between the gradient of the harmonic field on the boundary and the height of the profile at the same point. The correlation has been explicitly computed and shown to converge to a precise limit for persistent boundaries. Antipersistent profiles lead to a correlation coefficient that is dependent on the self-affinity range.

Finally we have shown that the same mapping can be used to address different boundary conditions, including the extreme case of a pointlike source on the boundary that is treated exactly.

Extensions of the above technique are numerous. We essentially focused here on static problems involving harmonic fields. However, the same mapping may also be used in connection with evolution problems such as diffusion or wave propagation (localization). Thermal diffusion in the vicinity of a rough boundary has recently been shown to display anomalous scaling behavior at early stages, which could be addressed by such methods. The ac impedence of rough electrodes is another potential field of extension that has been studied in recent years.

The mapping we discuss may also be one constitutive part of a different mapping dealing with different geometries. An example of such extensions is the stress intensity factor (i.e., the singular behavior of the stress field) at a crack tip. In the framework of antiplane elasticity one can compute the local stress intensity factor at the crack tip and relate it to the far-field singular behavior. This problem is currently being investigated.

In a companion paper [24] we extend our mapping to computations of biharmonic fields with applications to Stokes flow close to rough boundaries and elastic stress fields close to a rough surface.

## ACKNOWLEDGMENTS

It is a pleasure to acknowledge useful discussions with A. C. Boccara and F. Plouraboué. D.V. thanks the DRET for support. Partial support was also provided by the CNRS GdR ''Physique des Milieux Hétérogènes Complexes.''

[1] D. M. Kulawansa, L. C. Jensen, S. C. Langford, J. T. Dickinson, and Y. Watanabe, J. Mater. Res. **9**, 476 (1994).
[2] E. Guilloteau, Ph.D. dissertation, Universite Paris-Sud, 1995 (unpublished).
[3] B. B. Mandelbrot, *The Fractal Geometry of Nature* (Freeman, New York, 1982).
[4] J. Feder, *Fractals* (Plenum Press, New York, 1988).
[5] T. Halpin-Healy and Y.-C. Zhang, Phys. Rep. **254**, 215 (1995).
[6] P. Meakin, Phys. Rep. **235**, 189 (1993).
[7] A. L. Barabási and H. E. Stanley, *Fractal Concepts in Surface Growth* (Cambridge Univ. Press, Cambridge, 1995).
[8] T. Vicsek, *Fractal Growth Phenomena* (World Scientific, Singapore, 1992).
[9] D. E. Wolf, in *Scale Invariance, Interfaces and Non-equilibrium Dynamics*, edited by J. Vannimenus and D. E. Wolf (Plenum, New York, 1994).
[10] B. B. Mandelbrot, D. E. Passoja, and A. J. Paullay, Nature **308**, 721 (1984); S. R. Brown, Geophys. Res. Lett. **13**, 1430 (1986); R. H. Dauskardt, F. Haubensak, and R. O. Ritchie, Acta Metall. Mater. **38**, 143 (1990); B. L. Cox and J. S. Y. Wang, Fractals 1, **87** (1993); E. Bouchaud, G. Lapasset, and J. Planès, Europhys. Lett. **13**, 73 (1990); K. J. Måløy, A. Hansen, E. L. Hinrichsen, and S. Roux, Phys. Rev. Lett. **68**, 213 (1992).
[11] S. He, G. L. M. K. S. Kahanda, P. z. Wong, Phys. Rev. Lett. **69**, 3731 (1992), and references therein.
[12] L. Boyer, F. Houzé, A. Tonck, J. L. Loubet, and J-M Georges, J. Phys. D. 27, 1504 (1994).
[13] A. G. Voronovich, *Wave Scattering from Rough Surfaces* (Springer-Verlag, Berlin, 1994).
[14] D. Vandembroucq. A. C. Boccara, and S. Roux, Europhys. Lett. **30**, 209 (1995).

[15] A. E. Scheidegger, *The Physics of Flow through Porous Media* (University of Toronto, Toronto, 1974).
[16] R. W. Davidge, *Mechanical Behaviour of Ceramics* (Cambridge Univ. Press, Cambridge, 1979).
[17] F. M. Borodich, Int. J. Solids Structures **30**, 1513 (1993); F. M. Borodich and D. A. Onishchenko, J. Friction Wear **14**, 14 (1993).
[18] S. Roux, J. Schmittbuhl, J. P. Vilotte, and A. Hansen, Europhys. Lett. **23**, 277 (1993).
[19] P. Meakin and B. Sapoval, Phys. Rev. A **43**, 6 (1991); **43**, 2993 (1991).
[20] B. Sapoval, Ricardo Gutfraind, P. Meakin, M. Keddam, and H. Takenouti, Phys. Rev. E **48**, 5 (1993); **48**, 3333 (1993).
[21] T. C. Halsey and M. Leibig, Europhys. Lett. **14**, 8 (1991); **14**, 815 (1991).
[22] T. C. Halsey and M. Leibig, Phys. Rev. A **43**, 12 (1991); **43**, 7087 (1991).
[23] B. Sapoval, Phys. Rev. Lett. **73**, 24 (1994); **73**, 3314 (1994).
[24] D. Vandembroucq and S. Roux, following paper, Phys. Rev. E **55**, 6186 (1997).
[25] C. Pozrikidis, J. Fluid Mech. **180**, 495 (1987).
[26] J. J. L. Higdon, J. Fluid Mech. **159**, 195 (1985).
[27] C. Pozrikidis, J. Fluid Mech. **255**, 11 (1995).
[28] H. Hasimoto and O. Sano, Annu. Rev. Fluid Mech. **12**, 335 (1980).
[29] C. Pozrikidis, *Boundary Integral and Singularity Methods for Linearized Viscous Flow* (Cambridge University Press, Cambridge, 1992).
[30] P. Henrici, *Applied and Computational Complex Analysis* (Wiley, New York, 1985), Vol. III.
[31] M. H. Gutknecht, Numer. Math. **36**, 405 (1981); M. H. Gutknecht, SIAM J. Sci. Stat. Comput. **4**, 1 (1983).
[32] J. Schmittbuhl, J. P. Vilotte, and S. Roux, Phys. Rev. E **51**, 131 (1995).